Eur. Phys. J. C (2023) 83:846
https://doi.org/10.1140/epjc/s10052-023-12010-y

THE EUROPEAN PHYSICAL JOURNAL C

Regular Article - Theoretical Physics

A simulated search for the singlet vector-like bottom quark decaying into tW at high energy pp colliders

Jinzhong Han[1,a], **Liangliang Shang**[2], **Bingfang Yang**[2]

[1] School of Physics and Telecommunications Engineering, Zhoukou Normal University, Zhoukou 466001, China
[2] School of Physics, Henan Normal University, Xinxiang 453007, China

Received: 6 June 2023 / Accepted: 5 September 2023

Abstract In a framework of simplified model, we perform a simulated search for the singlet vector-like bottom quark B decaying into tW with t hadronic decay and W leptonic decay at the 14 TeV high-luminosity LHC (HL-LHC), 27 TeV high energy LHC (HE-LHC) and 100 TeV Future Circular Hadron Collider (FCC-hh). In this work, we focus on the case that the B only couples with the third generation quarks of the Standard Model. We make a detailed detector simulations of the signal and backgrounds and obtain the 2σ exclusion limit and 5σ discovery prospects. Our results show that the upcoming HL-LHC can exclude (discover) the m_B to 2100 (1900) GeV for a typical coupling strength $g^* = 0.2$. For the HE-LHC (FCC-hh), this exclusion capability on the B quark mass can be expanded to more than 3000 (5000) GeV.

Contents

1 Introduction

Though the vector-like quarks (VLQ) are not present in the Standard Model (SM), they naturally arise near the electroweak scale in many extensions of new physics, such as extra dimension [1], little Higgs [2], composite Higgs models [3], and so on. Unlike the chiral SM quarks, the left- and right-handed components of VLQ transform in the same way under the SM electroweak gauge group. Their mass terms do not originate from the Yukawa coupling to the SM Higgs field so that they can avoid the strict constraints on chiral quarks set by the Higgs boson data at the LHC. Moreover, the VLQs can provide an understanding of the W-mass anomaly [4,5] and the some of the open questions in the SM, as described in Ref. [6].

For the VLQs coupling to the SM ones with renormalizable interactions, there are seven gauge-covariant multiplets, that is two singlets $[(T), (B)]$, three doublets $[(X, T), (T, B), (B, Y)]$ and two triplets $[(X, T, B), (T, B, Y)]$, where the fields T, B, X, Y have electric charges $2/3$, $-1/3$, $5/3$, $-4/3$, respectively. At the hadron colliders, the VLQs can be single produced via the electroweak interaction or pair produced via the strong interaction. Compared with the QCD pair produced process, the electroweak VLQ single produced has weaker phase-space suppression so that it is very attractive in the VLQ high-mass regime. In recent literatures, the single production processes $bg \to B \to bZ$ [7], $bg \to B \to tW$ [8] and $qg \to B\bar{b}j \to bZ\bar{b}j$ [9] at the LHC, the production process $ep \to \nu_e B \to \nu_e bZ$ [10] at future ep colliders, and the production process $e^+e^- \to B\bar{b} \to tW^-\bar{b}$ [11] at future electron-positron colliders have been considered. In this work, we will consider the single production of the singlet B via $pp \to Bj \to tWj$ at the upcoming high-luminosity LHC (HL-LHC), the future high energy LHC (HE-LHC) and the Future Circular Hadron Collider (FCC-hh).

Experimentally, the relevant searches have been performed by the CMS and ATLAS collaborations at the LHC with 13TeV. The CMS collaboration performed a search for VLB pair production in the fully hadronic final state using LHC Run 2 data with 137 fb^{-1}, and set the lower limits on the VLB mass equal to 1570 GeV for $Br(B \to bH) = 100\%$,

[a] e-mail: hanjinzhong@zknu.edu.cn (corresponding author)

Published online: 22 September 2023

1390 GeV for $Br(B \to bZ) = 100\%$ and 1450 GeV for $Br(B \to bH) = Br(B \to bZ) = 50\%$. The ATLAS collaboration performed a search for VLB pair production with at least one leptonically decaying Z boson and a b quark using LHC Run 2 data with 139 fb^{-1} [12], and set the limits on the singlet (doublet) model at $m_B > 1.20$ (1.32) TeV. In the case of $Br(B \to bZ) = 100\%$, the limit is $m_B > 1.42$ TeV [13].

The paper is organized as follows: In Sect. 2, we review the effective Lagrangian including an $SU(2)$ singlet VLB; In Sect. 3, we give a detail analysis of the signal and backgrounds, and make a fast detector simulation on the single production of VLB decaying to tW at the HL-LHC, HE-LHC and FCC-hh; In Sect. 4, we summarize the discovery potentiality at different hadron colliders and give some discussions about the effect of pile-up.

2 The effective Lagrangian

We consider the case that the VLB is an $SU(2)$ singlet with charge $-1/3$, the Lagrangian parameterizing the VLQ-B couplings to quarks and electroweak bosons can be expressed as [14]:

$$\begin{aligned}\mathcal{L}_B = \frac{gg^*}{2}\Bigg\{&\sqrt{\frac{R_L}{1+R_L}}\frac{1}{\sqrt{2}}\left[\bar{B}_L W^-_\mu \gamma^\mu u_L\right]\\ &+\sqrt{\frac{1}{1+R_L}}\frac{1}{\sqrt{2}}\left[\bar{B}_L W^-_\mu \gamma^\mu t_L\right]\\ &+\sqrt{\frac{R_L}{1+R_L}}\frac{1}{2c_W}\left[\bar{B}_L Z_\mu \gamma^\mu d_L\right]\\ &+\sqrt{\frac{1}{1+R_L}}\frac{1}{2c_W}\left[\bar{B}_L Z_\mu \gamma^\mu b_L\right]\\ &-\sqrt{\frac{R_L}{1+R_L}}\frac{m_B}{2m_W}\left[\bar{B}_R H d_L\right]\\ &-\sqrt{\frac{1}{1+R_L}}\frac{m_B}{2m_W}\left[\bar{B}_R H b_L\right]\Bigg\} + h.c. \end{aligned} \quad (1)$$

where g is the $SU(2)_L$ gauge coupling constant and θ_W is the Weinberg angle, g^* is the coupling strength that parametrizes the single B production coupling associated with the SM quarks, R_L is the rate of the B quark decaying into the first and third generation quarks. In this work, we are interested in the case in which the VLQ-B only couplings to the third generation of SM quarks, that is $R_L = 0$, so that the Lagrangian can be re-expressed as:

$$\begin{aligned}\mathcal{L}_B = \frac{gg^*}{2}\Bigg\{&\frac{1}{\sqrt{2}}[\bar{B}_L W^-_\mu \gamma^\mu t_L] + \frac{1}{2\cos\theta_W}[\bar{B}_L Z_\mu \gamma^\mu b_L]\\ &-\frac{m_B}{2m_W}[\bar{B}_R H b_L] - \frac{m_b}{2m_W}[\bar{B}_L H b_R]\Bigg\} + h.c. \end{aligned} \quad (2)$$

Note that the coupling strength g^* is also described as κ_T or $\sin\theta_L$ in different literatures. By comparing these symbols [14], we obtain the relation as follows:

$$g^* = \sqrt{2}\kappa_B = 2\sin\theta_L \quad (3)$$

Here we take a conservative range for the coupling strength [15]: $g^* \leq 0.5$, which is consistent with the current experiment limits. Besides, the mass m_B can be set a lower limit at about 850 GeV for the singlet VLB branching fractions to $W : Z : H = 1{:}0{:}0$ coming from Fig. 19(c) of Ref. [15] and at about 650 GeV for the singlet VLB branching fractions to $W : Z : H = \frac{1}{2} : \frac{1}{4} : \frac{1}{4}$ coming from Fig. 19(d) of Ref. [15].

3 Detector simulation

In this section, we will focus on the background analysis and detector simulation at the high energy hadron colliders. For the colliders, we will consider the following options:

- HL-LHC with 3 ab^{-1} at $\sqrt{s} = 14$ TeV;
- HE-LHC with 15 ab^{-1} at $\sqrt{s} = 27$ TeV;
- FCC-hh with 30 ab^{-1} at $\sqrt{s} = 100$ TeV.

At the pp colliders, the single B can be produced by exchanging the weak gauge bosons W, Z and the Higgs boson. We show the Feynman diagram of this process at tree level in Fig. 1, where j involves the first two generation quarks. When $R_L = 0$, the VLB only couplings with the third generation quarks so that the contribution of the left diagram will vanish. Since the experiment has limited the R_L strongly, we take $R_L = 0$ in this work.

We calculated the leading order cross sections of the signal $pp \to Bj \to tW^-j$ by MadGraph5_aMC@NLO_v3.4.2 [17] with the parton distribution function (PDF) nn23nlo [18]. The input SM parameters are taken as follows [19]:

$$m_t = 172.76\ \text{GeV}, \quad m_Z = 91.1876\ \text{GeV},$$
$$m_H = 125.10\ \text{GeV}, \sin^2\theta_W = 0.231, \alpha(m_Z) = 1/128.$$

We show the cross sections as a function of m_B with $g^* = 0.2$ in Fig. 2, where the conjugate process $pp \to \bar{B}j \to \bar{t}W^+j$ has been included. We can see that the cross sections decrease rapidly as the increase of m_B due to the suppression of phase space.

In this work, we will explore the single B production through the following channel

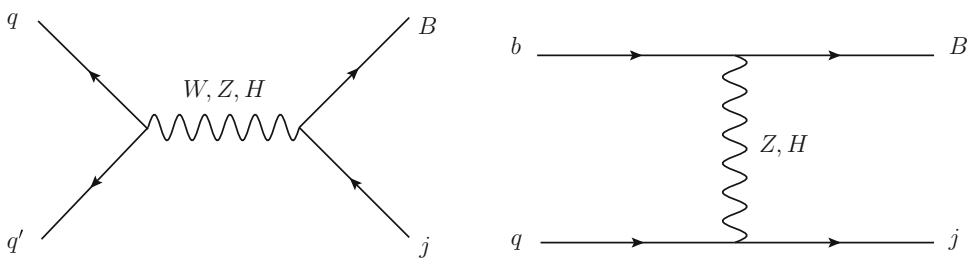

Fig. 1 Feynman diagrams for $pp \to Bj$ at the tree level

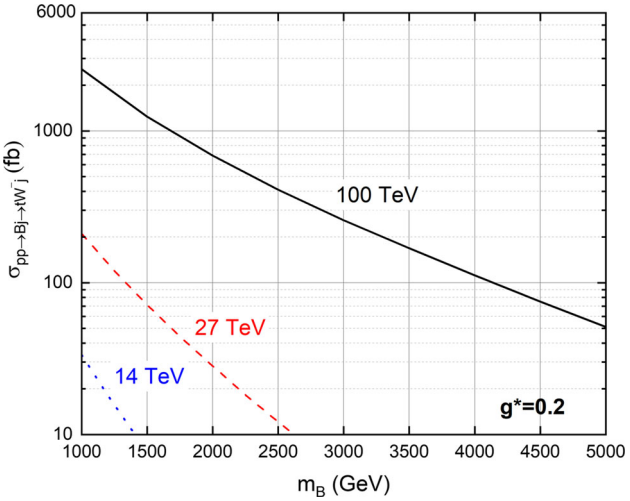

Fig. 2 Cross sections of the process $pp \to Bj \to tW^- j$ as a function of m_B for three colliders with $g^* = 0.2$, where the conjugate process $pp \to \bar{B} j \to \bar{t} W^+ j$ has been included

$$pp \to B(\to tW)j \to t(\to bjj)\, W(\to l\bar{\nu})j \to 3j + b + l + \not{E}_T$$

According to the feature of the signal, the dominant backgrounds come from $t\bar{t}$, single top production processes tj, tW, tb and tWj, tZj, and WWZ, WWH. For the SM backgrounds, we generate their tree-level cross sections and normalize them to the next-to-leading-order (NLO) or the next-to-next-to-leading order (NNLO) cross sections by considering a K factor, which is shown in Table 1.

In order to investigate the observability of the signal, it is necessary to make a detailed detector simulation. We generate the parton-level events of the signal and backgrounds by MadGraph5_aMC@NLO_v3.4.2 with the PDF nn23nlo. Then, we transmit these parton-level events to Pythia [23] for showering and hadronization. We make a fast detector simulation via Delphes 3.14 [24] and cluster jets by Fastjet [25] using the anti-kt algorithm with a cone radius of $R = 0.8$ and the momentum parameter $JetPTMin = 200$ GeV [26].

Finally, we use MadAnalysis 5 [27] to analyze the events. In our simulation, the conjugate processes of signal and backgrounds have been included. According to the features of signal and backgrounds, we take lepton number $N_l = 1$ and b-jet number $N_b = 1$ as the trigger condition.

The basic cuts at parton level for the signal and backgrounds are taken as follows:

$$\begin{aligned} &\Delta R(x, y) > 0.4 && x, y = \ell,\ j,\ b \\ &p_T^{\ell} > 25\ \text{GeV}, && |\eta_{\ell}| < 2.5 \\ &p_T^{j} > 25\ \text{GeV}, && |\eta_{j}| < 5.0 \\ &p_T^{b} > 25\ \text{GeV}, && |\eta_{b}| < 5.0 \end{aligned}$$

In order to analyze the observability, we evaluate the signal significance by using the Poisson formula as follows [28]:

$$SS = \sqrt{2L[(\sigma_S + \sigma_B)\ln(1 + \frac{\sigma_S}{\sigma_B}) - \sigma_S]} \tag{4}$$

where L is the integrated luminosity and σ_S, σ_B are the signal and background cross sections after all cuts, respectively. Here, the exclusion significance corresponds to $SS = 2$ and the discovery significance corresponds to $SS = 5$. In the next content, we will show the exclusion and discovery significance of the signal at different colliders.

3.1 HL-LHC

For the signal, the W boson and the top quark are boosted highly since they come from the decay of the heavier B quark. As a result, the missing energy and the transverse momentum of the lepton from the decay of W boson are much larger than that in the backgrounds. Meanwhile, the decay products of the top quark and W boson are collimated and captured in two large-radius (large-R) jets. So, we choose the missing energy $\not{E}_T$, transverse momentum p_T^l and the mass M_{j_1} as selection criterias and show these distributions in Fig. 3. In the signal distribution of M_{j_1}, we can see that there are two peaks, one is at $\sim m_W$ and the other is at $\sim m_t$, which

Table 1 The K-factors of higher-order corrections for the backgrounds

Process	$t\bar{t}$	tj	tW	$t\bar{b}$	tWj	tZj	WWZ	WWH
K-factor	1.8 [20]	1.4 [21,22]	1.6 [21,22]	1.9 [21,22]	1.6	1.0 [17]	1.7 [17]	1.3 [17]

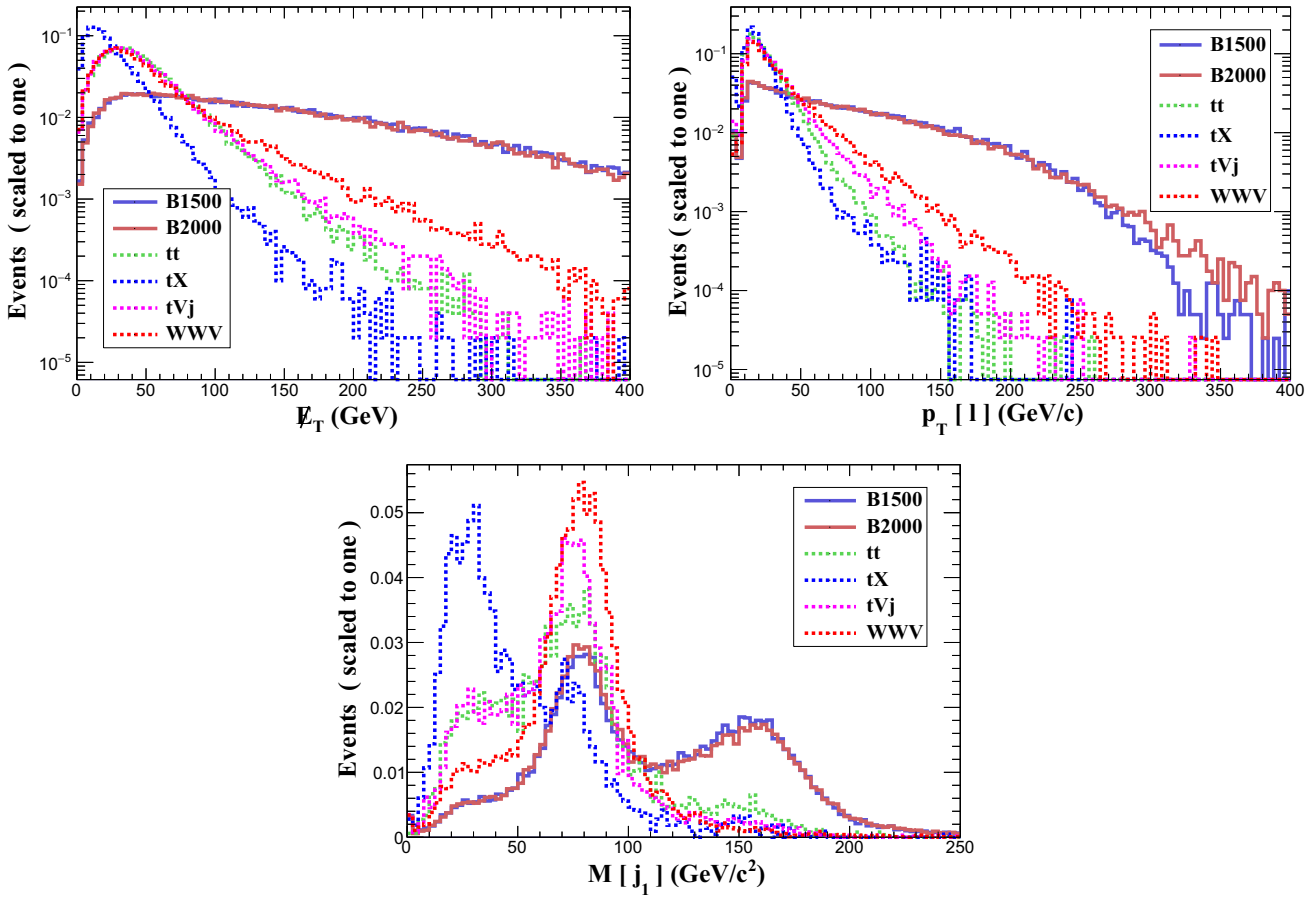

Fig. 3 Normalized distributions of $\not{E}_T$, p_T^l and M_{j_1} for the two signal benchmark points and backgrounds with $g^* = 0.2$ at $\sqrt{s}$ = 14 TeV

Table 2 Cut flow of the two signal benchmark points (B1500, B2000) and backgrounds $tX(X = W, j, \bar{b})$, $tVj(V = W, Z)$, $WWV(V = Z, H)$ at the 14 TeV LHC with $g^* = 0.2$. Here, S/B denotes the signal-to-noise ratio and "–"denotes that the cross section is negligible

Cuts	Signals (fb)		Backgrounds (fb)				S/B	
	1500 GeV	2000 GeV	$t\bar{t}$	tX	tVj	WWV	1500 GeV	2000 GeV
Basic cuts	6.04E−01	8.41E−02	5.11E+04	1.11E+05	3.97E+03	6.03E+00	3.64E−6	5.06E−7
$N(l) = 1, N(b) = 1$	1.71E−01	2.27E−02	1.22E+03	2.93E+02	7.61E+01	1.71E−01	1.07E−4	1.42E−5
$\not{E}_T > 220$ GeV	7.32E−02	9.81E−03	7.05E+01	1.56E+01	4.52E+00	1.77E−02	8.08E−4	1.08E−5
$p_T^l > 260$ GeV	2.22E−02	3.07E−03	–	–	3.97E−01	1.09E−03	5.57E−2	7.72E−3
130 GeV< M_{j_1} <180 GeV	1.25E−02	1.73E−03	–	–	–	1.21E−04	1.03E+2	1.43E+1

come from the constructed large-R jets. We take $\not{E}_T > 220$ GeV, $p_T^l > 260$ GeV, 130 GeV< M_{j_1} <180 GeV as cuts and summarize the cut flows of the two signal benchmark points (B1500, B2000) and the backgrounds for $g^* = 0.2$ in Table 2. In the last column of the Table 2, we also show the signal-to-noise ratio S/B. After the selected cuts, the total cut efficiency of signal can reach 2.07% (2.06%) for m_B = 1500(2000) GeV and the total ratio S/B can be improved efficiently. We scan the parameter space $g^* \in [0.1, 0.5]$ and $m_B \in [1000\,\text{GeV}, 2500\,\text{GeV}]$ and impose the average value 2.07% of these two signal efficiencies to all the parameter space.

In Fig. 4, we show the 2σ exclusion and 5σ discovery capabilities on the $g^* - m_B$ plane at the $\sqrt{s} = 14$ TeV. We can see that the B quark mass below 1750 (1300) GeV can be excluded at the 2σ level for the typical coupling strength $g^* = 0.5(0.2)$ values corresponding to 100 fb^{-1}. If the integrated luminosity of 3000 fb^{-1} can be reached, the B quark can be excluded (discovered) with a mass larger than 2400 GeV for $g^* > 0.3(0.4)$.

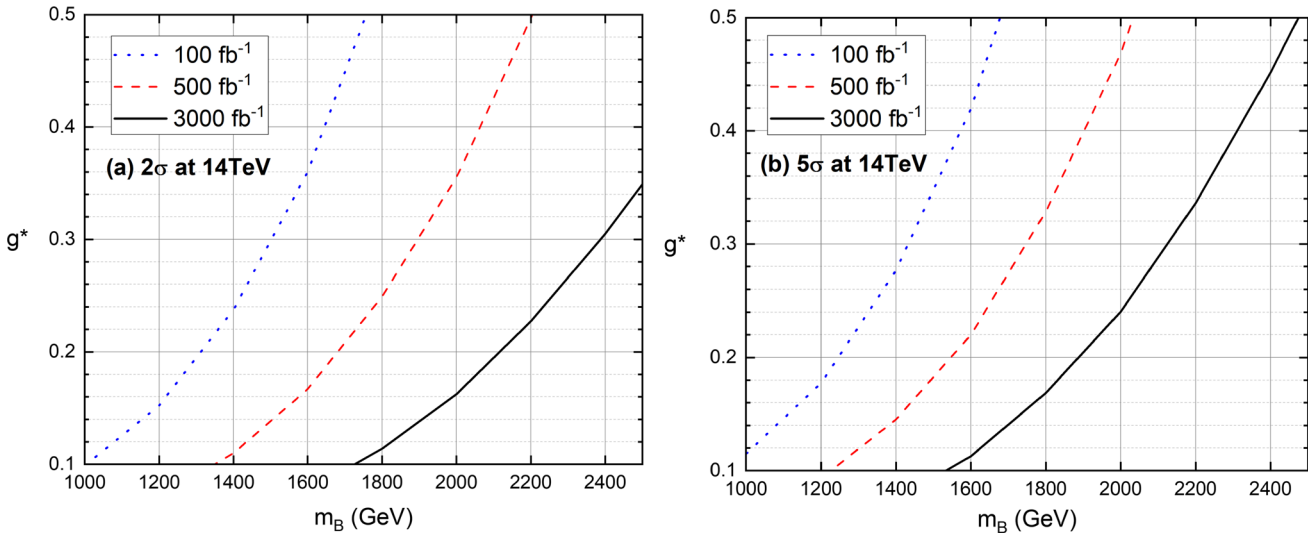

Fig. 4 Exclusion limit (at 2σ) and discovery prospect (at 5σ) for the signal on $g^* - m_B$ planes at 14 TeV LHC with three typical luminosities

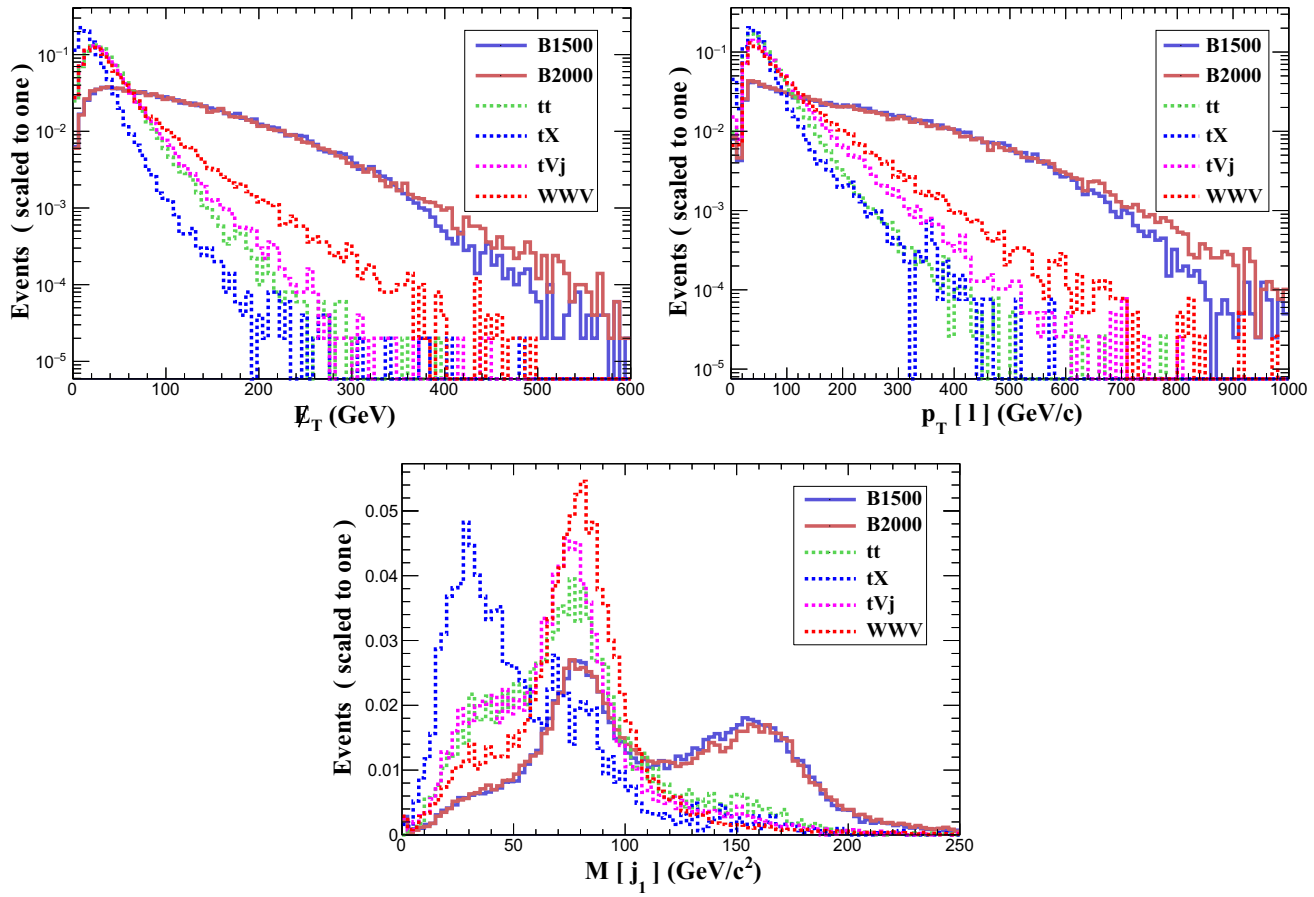

Fig. 5 Normalized distributions of $\not{E}_T$, p_T^l and M_{j_1} for the two signal benchmark points and backgrounds with $g^* = 0.2$ at $\sqrt{s} = 27$ TeV

Table 3 Same as Table 2, but for $\sqrt{s} = 27$ TeV

Cuts	Signals (fb)		Backgrounds (fb)				S/B	
	1500 GeV	2000 GeV	$t\bar{t}$	tX	tVj	WWV	1500 GeV	2000 GeV
Basic cuts	5.23E+00	9.90E−01	1.92E+05	3.19E+05	1.75E+04	1.52E+01	9.9E−6	1.87E−6
$N(l) = 1, N(b) = 1$	1.47E+00	2.70E−01	6.09E+03	1.26E+03	4.99E+02	5.68E−01	1.87E−4	3.43E−5
$\not{E}_T > 375$ GeV	2.33E−01	4.38E−02	2.69E+01	2.55E+01	3.84E+00	1.46E−02	4.15E−3	7.79E−3
$p_T^l > 220$ GeV	6.91E−02	1.64E−02	–	6.37	3.49E−01	2.13E−03	1.03E−2	2.44E−3
130GeV< M_{j_1} <180GeV	3.43E−02	7.70E−03	–	–	–	3.05E−04	1.12E+2	2.53E+1

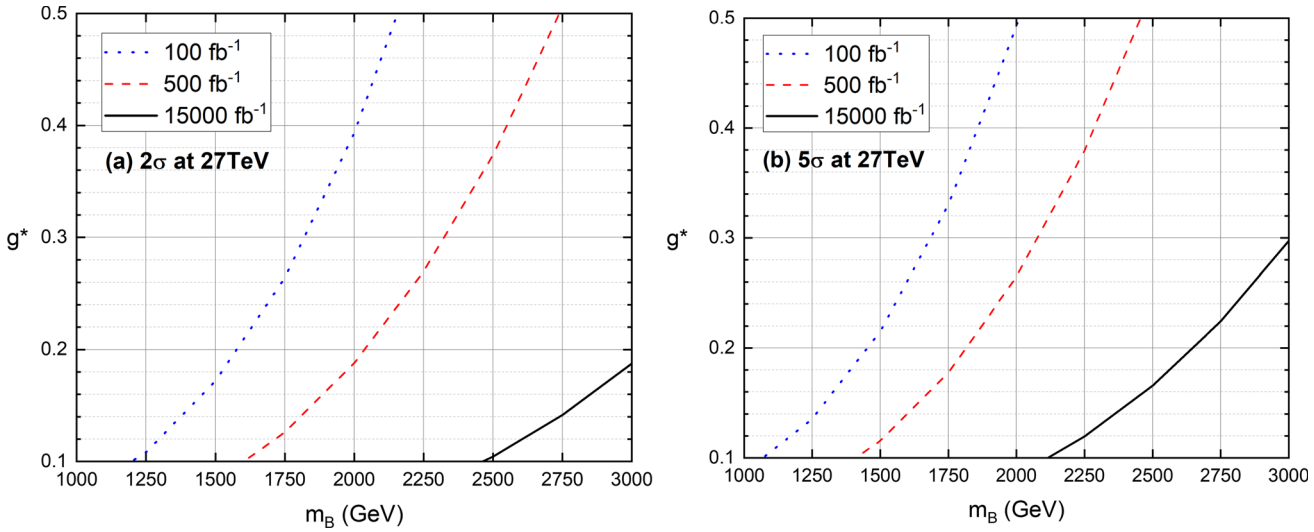

Fig. 6 Same as Fig. 4 but for 27 TeV

3.2 HE-LHC

In this case, we also choose the missing energy $\not{E}_T$, transverse momentum p_T^l and the mass M_{j_1} as selection criterias to suppress the backgrounds. We show these distributions in Fig. 5 and can see that the two constructed large-R jets in the signal distribution of M_{j_1}. We take $\not{E}_T > 375$ GeV, $p_T^l > 220$ GeV and 130 GeV $< M_{j_1} <$ 180 GeV as cuts and summarize the cut flows in Table 3. We can see that the total cut efficiency of signal can reach 0.66% (0.78%) for $m_B = 1500(2000)$ GeV, and the total signal-to-noise ratio S/B are improved efficiently. Same as the LHC, we scan the parameter space $g^* \in [0.1, 0.5]$ and $m_B \in [1000\,\text{GeV}, 3000\,\text{GeV}]$ and impose the average value 0.72% of these two signal efficiencies to all the parameter space at HE-LHC.

In Fig. 6, we shows the exclusion and discovery capabilities on the $g^* - m_B$ plane at $\sqrt{s} = 27$ TeV. Compared to the HL-LHC, we can see that the B quark mass below 2150 (1600) GeV can be excluded at the 2σ level for the typical coupling strength $g^* = 0.5(0.2)$ corresponding to 100 fb^{-1}. If the high integrated luminosity of 15ab^{-1} can be reached, the B quark can be excluded (discovered) with a mass larger than 3000 GeV for $g^* > 0.2(0.3)$.

3.3 FCC-hh

In this case, we choose the transverse momentum p_T^b as selection criteria except for the missing energy $\not{E}_T$, transverse momentum p_T^l and the mass M_{j_1}. We show these distributions in Fig. 7 and take $\not{E}_T > 360$ GeV, $p_T^l > 220$ GeV and $p_T^b > 450$ GeV as cuts. We summarize the cut flows of the two signal benchmark points (B1500, B2000) and the backgrounds for $g^* = 0.2$ in Table 4. We can see that the total cut efficiency of the signal can reach 0.67% (0.65%) for $m_B = 1500(2000)$ GeV, the total signal-to-noise ratio S/B can be enhanced greatly. Similarly, we scan the parameter space $g^* \in [0.1, 0.5]$ and $m_B \in [1000\,\text{GeV}, 5000\,\text{GeV}]$ and impose the average value 0.66% of these two signal efficiencies to all the parameter space at FCC-hh.

We show the exclusion and discovery capabilities in $g^* - m_B$ plane at $\sqrt{s} = 100$ TeV in Fig. 8. Corresponding to 100 fb^{-1}, we can see that the B quark mass below 3660 (2600) GeV can be excluded at the 2σ level for the typi-

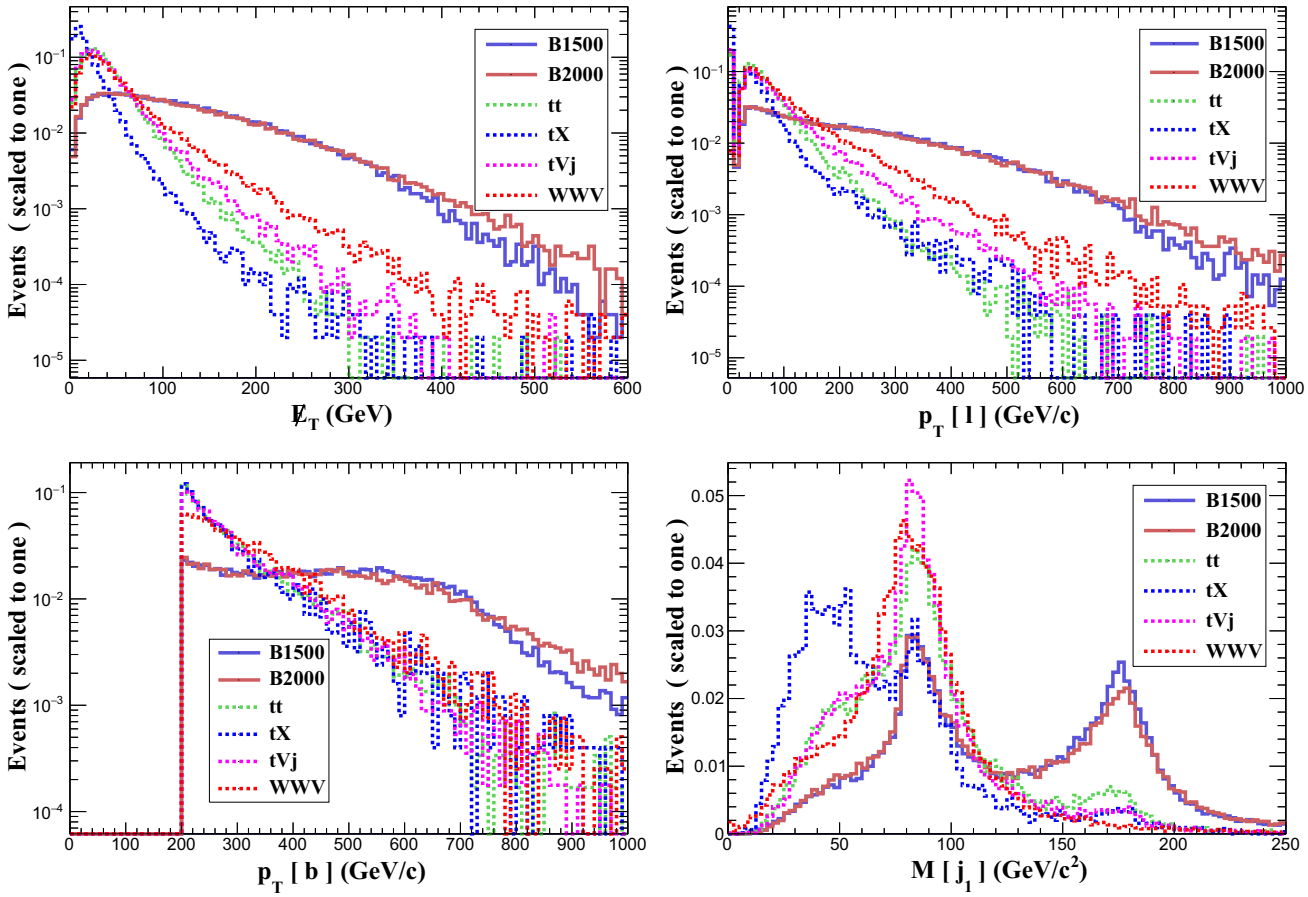

Fig. 7 Normalized distributions $\not{E}_T$, p_T^l, p_T^b and M_{j_1} for the two signal benchmark points and backgrounds with $g^* = 0.2$ at $\sqrt{s} = 100$ TeV

Table 4 Same as Table 2, but for $\sqrt{s} = 100$ TeV

Cuts	Signals (fb)		Backgrounds (fb)				S/B	
	1500 GeV	2000 GeV	$t\bar{t}$	tX	tVj	WWV	1500 GeV	2000 GeV
Basic cuts	7.84E+01	1.97E+01	1.56E+06	1.71E+06	1.71E+05	6.87E+01	2.28E−5	5.72E−6
$N(l) = 1, N(b) = 1$	2.62E+01	6.22E+00	1.08E+05	2.84E+04	1.14E+04	3.57E+00	1.77E−4	4.22E−5
$\not{E}_T > 360$ GeV	5.13E+00	1.27E+00	1.06E+03	5.46E+02	1.71E+02	1.32E−01	2.89E−3	7.17E−4
$p_T^l > 220$ GeV	1.70E+00	4.87E−01	1.56E+02	2.39E+02	3.76E+01	2.34E−02	3.97E−3	1.13E−3
$p_T^b > 450$ GeV	1.44E+00	4.10E−01	3.12E+01	1.02E+02	1.71E+01	1.10E−02	9.59E−2	2.73E−3
140GeV< M_{j_1} <180GeV	5.29E−01	1.28E−01	–	–	–	1.37E−03	3.84E+2	9.33E+1

cal coupling strength $g^* = 0.5(0.2)$. If the high integrated luminosity of 30 ab^{-1} can be reached, the B quark can be excluded (discovered) with a mass larger than 5000 GeV for the coupling strength $g^* > 0.2(0.3)$.

4 Summary

In this paper, we studied the single production of B quark in the tW channel with the subsequent decay $t \to bjj$ and $W \to l\bar{\nu}$ at the HL-LHC, HE-LHC and FCC-hh. Based on a simplified model including an $SU(2)$ singlet B, we focused on the case that the B only couples with the third generation SM quarks. Considering the current theoretical and experimental constraints, we performed a detailed detector simulation and obtained the constraints on the parameter space $g^* - m_B$ at these colliders. Our results can provide a promising scheme to search for the VLB in the tW channel at the upcoming 14 TeV HL-LHC. For the 27TeV HE-LHC and 100TeV FCC-hh, they will provide the stronger exclusion and discovery capabilities to the VLB with higher integrated luminosities.

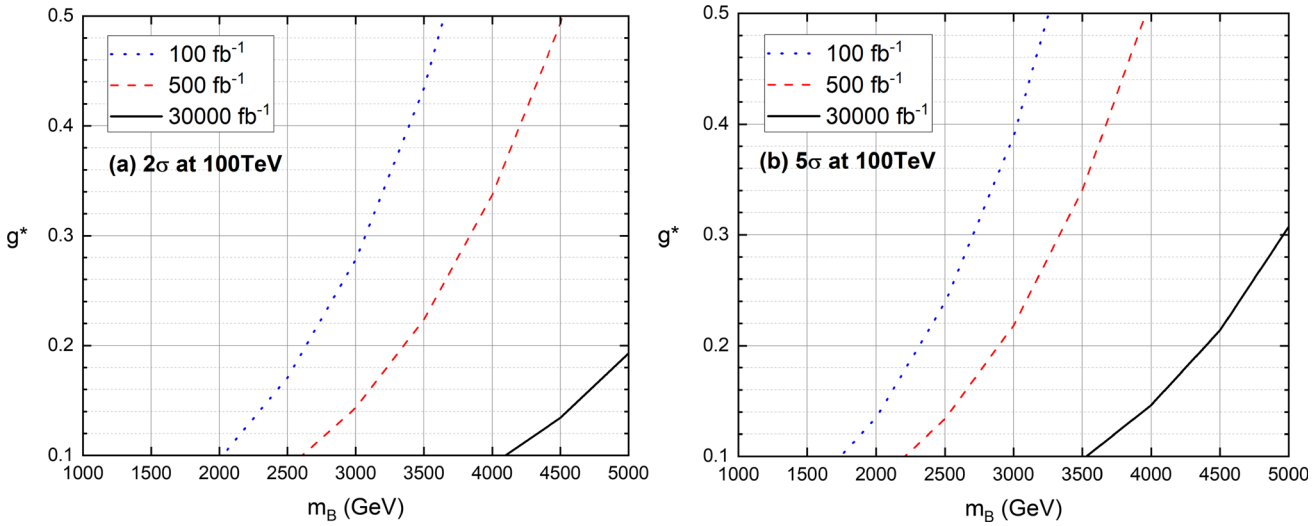

Fig. 8 Same as Fig. 4 but for 100 TeV

Besides, we discuss the impact of pile-up effect on our results. We know that the pile-up will be a big effect in the high energy hadron colliders and the jet shapes are particularly sensitive to the pile-up [29]. In recent years, some techniques using jet substructure [30–32] and other methods have been developed to mitigate this effect [33–35]. It is worth noting that the pile-up has large impact on the low-p_T regions while has little impact on the high-p_T regions [36]. The certain well-designed jet grooming procedures can significantly reduce the impact of pile-up, which can be referred to Fig. 4 of Ref. [37], where the p_T value is at least 300 GeV. For our cases, we construct the large-R jet or fat-jet with the momentum parameter $JetPTMin = 200$ GeV. Based on the discussions above, we expect that the pile-up will have little impact on our results, but this is only true if the substructure techniques or other methods are applied. A detailed simulation and discussion of the pipe-up will be carried out in our future work.

Acknowledgements This work is supported by the Natural Science Foundation of Henan Province under Grant No. 232300421217, the National Research Project Cultivation Foundation of Henan Normal University under Grant No. 2021PL10, and also powered by the High Performance omputing Center of Henan Normal University.

Data availability statement This manuscript has no associated data or the data will not be deposited. [Authors' comment: All data has been included in the tables and figures.]

Funded by SCOAP[3]. SCOAP[3] supports the goals of the International Year of Basic Sciences for Sustainable Development.

References

1. K. Agashe, G. Perez, A. Soni, Phys. Rev. D **75**, 015002 (2007)
2. N. Arkani-Hamed, A.G. Cohen, E. Katz, A.E. Nelson, JHEP **07**, 034 (2002)
3. M. Low, A. Tesi, L.T. Wang, Phys. Rev. D **91**, 095012 (2015)
4. J.J. Cao, L. Meng, L.L. Shang, S.Y. Wang, B.F. Yang, Phys. Rev. D **106**, 055042 (2022)
5. A. Crivellin, M. Kirk, T. Kitahara, F. Mescia, Phys. Rev. D **106**, L031704 (2022)
6. G. C. Branco, M. N. Rebelo, arXiv:2208.07235 [hep-ph]
7. X. Gong, C.X. Yue, Y.C. Guo, Phys. Lett. B **793**, 175–180 (2019)
8. J.Z. Han, Y.B. Liu, L. Xing, S. Xu, Chin. Phys. C **46**(10), 103103 (2022)
9. J.Z. Han, J. Yang, S. Xu, H.K. Wang, Nucl. Phys. B **975**, 115672 (2022)
10. L.L. Shang, C.P. Chen, S.Y. Wang, B.F. Yang, Nucl. Phys. B **984**, 115977 (2022)
11. L. Han, J.F. Shen, Y.B. Liu, Eur. Phys. J. C **82**, 637 (2022)
12. A.M. Sirunyan et al., CMS Collaboration. Phys. Rev. D **102**, 112004 (2020)
13. ATLAS Collaboration, ATLAS-CONF-2021-024
14. M. Buchkremer, G. Cacciapaglia, A. Deandrea, L. Panizzi, Nucl. Phys. B **876**, 376–417 (2013)
15. A. Buckley, J.M. Butterworth, L. Corpe, D. Huang, P. Sun, SciPost Phys. **9**(5), 069 (2020)
16. J.M. Campbell, R.K. Ellis, Phys. Rev. D **60**, 113006 (1999)
17. J. Alwall et al., JHEP **07**, 079 (2014)
18. J. Pumplin, A. Belyaev, J. Huston, D. Stump, W.K. Tung, JHEP **02**, 032 (2006)
19. P.A. Zyla et al. (Particle Data Group), Prog. Theor. Exp. Phys. **2020**, 083C01 (2020)
20. M. Czakon, A. Mitov, JHEP **12**, 054 (2012)

21. N. Kidonakis, arXiv:1808.02934 [hep-ph]
22. E. Boos, L. Dudko, Int. J. Mod. Phys. A **27**, 1230026 (2012)
23. T. Sjostrand, S. Mrenna, P.Z. Skands, JHEP **05**, 26 (2006)
24. J.D. Favereau et al., JHEP **02**, 57 (2014)
25. M. Cacciari, G.P. Salam, G. Soyez, Eur. Phys. J. C **72**, 1896 (2012)
26. Y.L. Dokshitzer, G.D. Leder, S. Moretti, B.R. Webber, JHEP **08**, 001 (1997)
27. E. Conte, B. Fuks, G. Serret, Comput. Phys. Commun. **184**, 222 (2013)
28. G. Cowan, K. Cranmer, E. Gross, O. Vitells, Eur. Phys. J. C **71**, 1554 (2011)
29. G. Soyez, G.P. Salam, J.H. Kim, S. Dutta, M. Cacciari, Phys. Rev. Lett. **110**(16), 162001 (2013)
30. R. Kogler et al., Rev. Mod. Phys. **91**(4), 045003 (2019)
31. P. Baldi, K. Bauer, C. Eng, P. Sadowski, D. Whiteson, Phys. Rev. D **93**(9), 094034 (2016)
32. D. Krohn, M. Low, M.D. Schwartz, L.-T. Wang, Phys. Rev. D **90**(6), 065020 (2014)
33. J.A. Martinez, O. Cerri, M. Pierini, M. Spiropulu, J.-R. Vlimant, Eur. Phys. J. Plus **134**(7), 333 (2019)
34. J. Monk, C. Wiglesworth, P. Hansen, arXiv:1812.07412 [hep-ph]
35. P.T. Komiske, E.M. Metodiev, B. Nachman, M.D. Schwartz, JHEP **12**, 051 (2017)
36. A. Avetisyan et al., arXiv:1308.1636 [hep-ex]
37. A. Altheimer et al., J. Phys. G **39**, 063001 (2012)